

## Supplementary

### Influence of crystalline phase on electrocatalytic behaviour for $\text{Sm}_{2-x}\text{Sr}_x\text{NiO}_{4-\delta}$ ( $x = 0.4$ to $1.0$ ) Ruddlesden Popper based system: A comparative study of bulk and thin electrocatalysts

Manisha Chauhan, Pardeep K. Jha, Priyanka A. Jha\* and Prabhakar Singh\*

Indian Institute of Technology (BHU), Varanasi, UP, India.

E-mail: [priyankajha.dce@gmail.com](mailto:priyankajha.dce@gmail.com), [psingh.app@iitbhu.ac.in](mailto:psingh.app@iitbhu.ac.in)

Table S1 Molar ratio of the chemicals used for the synthesis of $\text{Sm}_{2-x}\text{Sr}_x\text{NiO}_{4-\delta}$ ( $x = 0.4-1$ at the steps of 0.2)					
Sample Phases	Elements	0.4 (1gm)	0.6(1gm)	0.8(1gm)	1.0(1gm)
Bulk	$\text{Sm}_2\text{O}_3$	0.6739	0.5970	0.5185	0.4379
	$\text{SrCO}_3$	0.1434	0.2186	0.2952	0.3736
	$\text{NiO}$	0.1821	0.1844	0.1867	0.1891
Thin Film	$\text{Sm}_2\text{O}_3$		0.5970		0.4379
	$\text{SrCO}_3$		0.2186		0.3736
	$\text{NiO}$		0.1844		0.1891

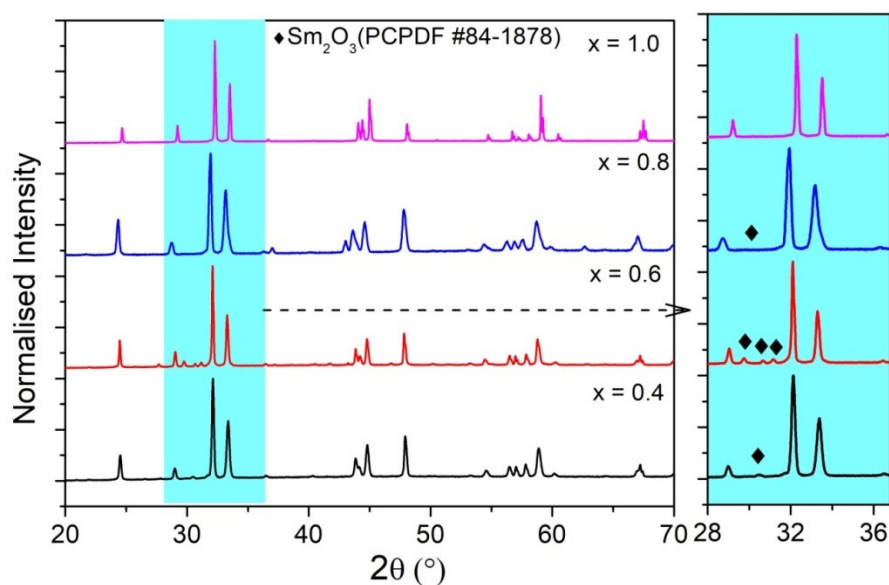
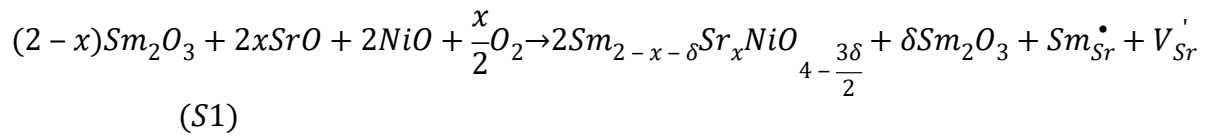


Fig.S1 depicts the X-ray diffractograms of the sintered pellets of  $\text{Sm}_{2-x}\text{Sr}_x\text{NiO}_{4-\delta}$  ( $x = 0.4-1$  at the steps of 0.2) samples (Right panel) shows the formation of secondary phase.

Fig.S1 depicts the X-ray diffractograms of the sintered pellets of  $\text{Sm}_{2-x}\text{Sr}_x\text{NiO}_{4-\delta}$  ( $x = 0.4$  to  $1$  at the steps of  $0.2$ ) samples. The samples are observed in a single phase with some extra peaks indexed in the right part of Fig.S1. These other peaks correspond to  $\text{Sm}_2\text{O}_3$  according to PCPDF # 84-1878. With the increase in SrO,  $\text{Sm}_2\text{O}_3$  remains as an unreacted precursor up to  $x = 0.6$ . Thereafter, it diminishes and at  $x = 1$ , the compound is pure phase and the mechanism can be illustrated in the equation (1)



It can be seen that there is splitting in the peak corresponding to  $2\theta \sim 44^\circ$  at  $x = 0.4$  and this splitting is converting into two peaks at  $x = 0.8$  and  $1.0$ . The individual peak corresponding to  $2\theta \sim 59^\circ$  at  $x = 0.4$  is splitting at  $x = 1.0$ . Also, the individual peak at  $2\theta \sim 48^\circ$  is observed to split at  $x = 1.0$ . These observations bring to quest regarding any phase conversion with  $x$ .

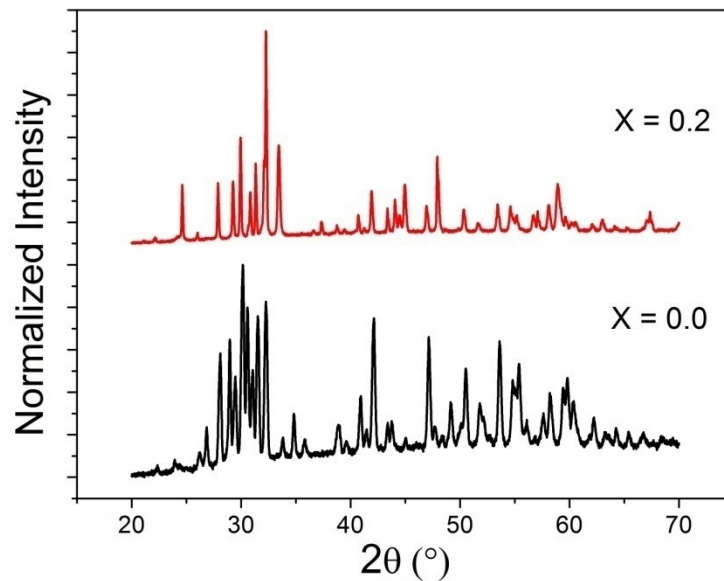


Fig.S2 depicts the X-ray diffractograms of the sintered pellets of  $\text{Sm}_{2-x}\text{Sr}_x\text{NiO}_{4-\delta}$  ( $x = 0.0$  and  $0.2$ )

Table S2 Atomic positions and R-factors obtained after refinement for the  $\text{Sm}_{2-x}\text{Sr}_x\text{NiO}_{4-\delta}$  ( $x = 0.4$  to  $1.0$ )

samples							
Sample	Atoms	Position coordinates			Occupancy	R-factors	
		x	Y	z		Bragg	$R_f$
						R-factor	factor
x = 0.4	Sm	0	0	0.36168	1.00000	7.14	5.51
	Sr	0	0	0.36180	1.00000		
	Ni	0	0	0	1.01078		
	O1	0.25	0.25	0	1.21120		
	O2	0	0	0.16217	0.85617		
x = 0.6	Sm	0	0	0.36165	1.00000	6.54	4.57
	Sr	0	0	0.36165	1.00000		
	Ni	0	0	0	1.01078		
	O1	0.25	0.25	0	0.75451		
	O2	0	0	0.15946	0.85617		
x = 0.8	Sm	0	0	0.36153	0.99993	3.68	2.37
	Sr	0	0	0.36153	1.00027		
	Ni	0	0	0	0.99605		
	O1	0.5	0	0	1.15618		
	O2	0	0	0.16544	0.89694		
x = 1.0	Sm	0	0	0.36151	0.90116	6.80	4.20
	Sr	0	0	0.36151	1.04018		
	Ni	0	0	0	1.27142		
	O1	0.5	0	0	1.00215		
	O2	0	0	0.16083	1.04720		

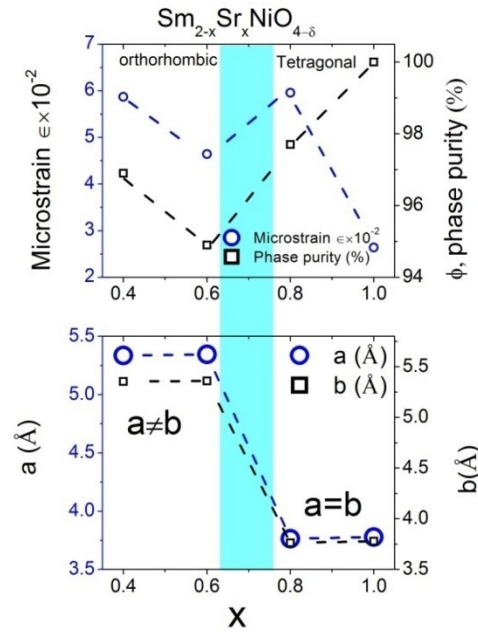


Fig.S3(a) Variation of microstrain and phase purity with x for the studied samples  $\text{Sm}_{2-x}\text{Sr}_x\text{NiO}_{4-\delta}$  ( $x = 0.4-1.0$  at the steps of 0.2). (b) Lattice parameters obtained from Rietveld refinement of the X-ray diffractograms.

The X-ray diffractograms showed the presence of some extra peaks . Thus, the phase purity of all the samples is determined by the formula:

$$\phi_{purity} = \frac{I_p}{I_p + 0.8I_s} \quad (S2)$$

where  $I_p$  represents the maximum intensity of primary peak and  $I_s$  represents the maximum intensity of the secondary phase. The phase purity is depicted in Fig. S3 (a). From the graph it is clear that the phase purity decreases with Sr substitution up to  $x = 0.6$  and thereafter, it increases to 100% for  $x = 1.0$ . The Microstrain caused by crystalline defects has been calculated from Rietveld refinement of XRD results by using Williamson–Hall model. The Williamson– Hall model is

given by  $\beta \cos\theta = 0.9 \frac{\lambda}{t} + 4 \epsilon \sin\theta$  where t is average crystallite size and  $\epsilon$  is microstrain,  $\beta$  is the full width at half maxima (FWHM) at Bragg's angle ( $2\theta$ ) and  $\lambda$  being the X-ray wavelength of Cu  $K\alpha$  ( $k = 1.54098 \text{ \AA}$ ). The slope and intercept of  $\beta \cos\theta$  vs  $4 \sin\theta$  curve (graph not shown here) gives the value of microstrain and crystallite size, respectively. Fig.

S3(a) shows the variation of microstrain with  $x$ . It is observed that the value of microstrain decreases with  $x$  for  $x = 0.4$  and  $0.6$  in orthorhombic region. Further, with the phase change, from  $x = 0.6$  to  $0.8$ , it increases from orthorhombic to tetragonal (illustrated through cyan rectangle in Fig. S3(a)) and further decreases with  $x = 1.0$ . Thus, the behavior of microstrain resembles the phase transition behavior. Fig.S3(b) shows the variation of lattice parameters obtained after Rietveld refinement of the X-ray diffractograms with  $x$ . It is observed that the lattice parameters  $a$  ( $5.33 \text{ \AA}$ )  $\neq$   $b$  ( $5.35 \text{ \AA}$ ) for the orthorhombic phase and for tetragonal phase  $a$  ( $3.76 \text{ \AA}$ ) =  $b$  ( $3.76 \text{ \AA}$ ).

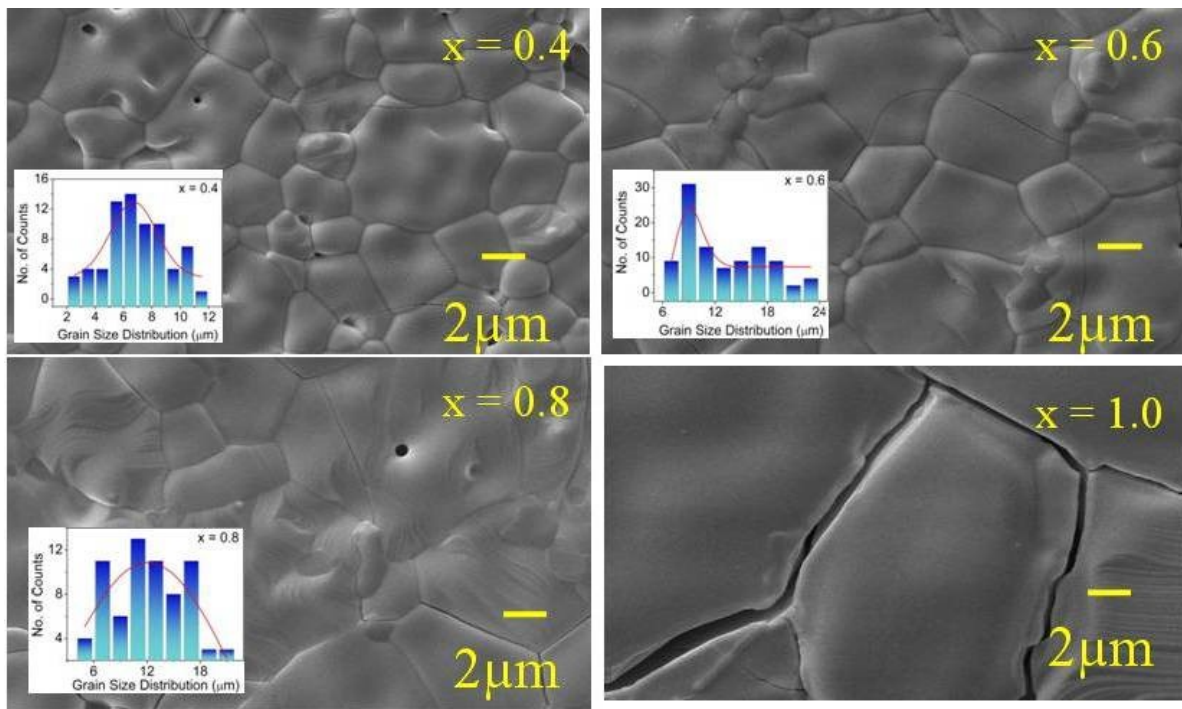


Fig. S4 SEM micrographs and their respective insets depict the grain size histograms for the bulk  $\text{Sm}_{2-x}\text{Sr}_x\text{NiO}_{4-\delta}$  ( $x = 0.4 - 1.0$  at the steps of 0.2)

The microstructure and chemical composition of the  $\text{Sm}_{2-x}\text{Sr}_x\text{NiO}_{4-\delta}$  ( $x = 0.4 - 1$  at the steps of 0.2) samples are characterized by SEM and EDX analysis. Fig. S5a represents the SEM micrograph and their respective insets depict the grain size histograms for the studied samples. With the increase in  $x$ , the grain size is observed to increase. The features observed at the surface indicate the grain –growth stage (highly densified) of the studied samples. The EDX data of all samples show

the presence of Sm, Sr, Ni, and Oxygen verifying the fact that the compound obtained is in stoichiometric compositions.

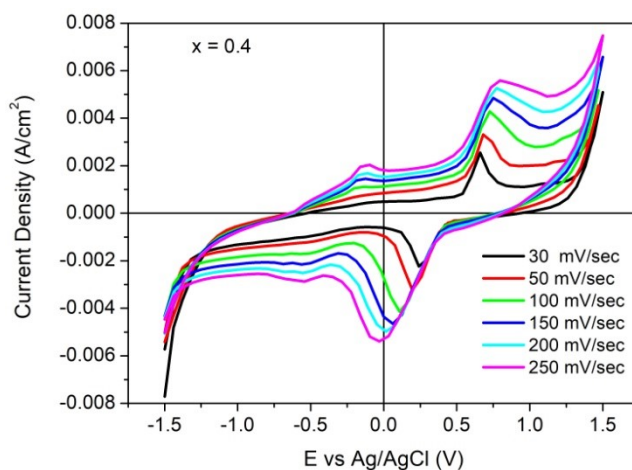


Fig.S5 Cyclic Voltammograms with the scan rate of the bulk  $\text{Sm}_{2-x}\text{Sr}_x\text{NiO}_{4-\delta}$  ( $x = 0.4$ ).

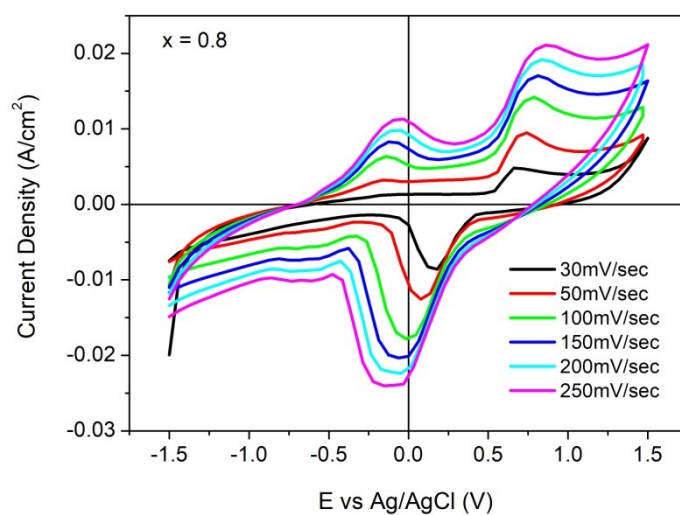


Fig.S6 Cyclic Voltammograms with the scan rate of the bulk  $\text{Sm}_{2-x}\text{Sr}_x\text{NiO}_{4-\delta}$  ( $x = 0.8$ ).

## Structural studies of thin film

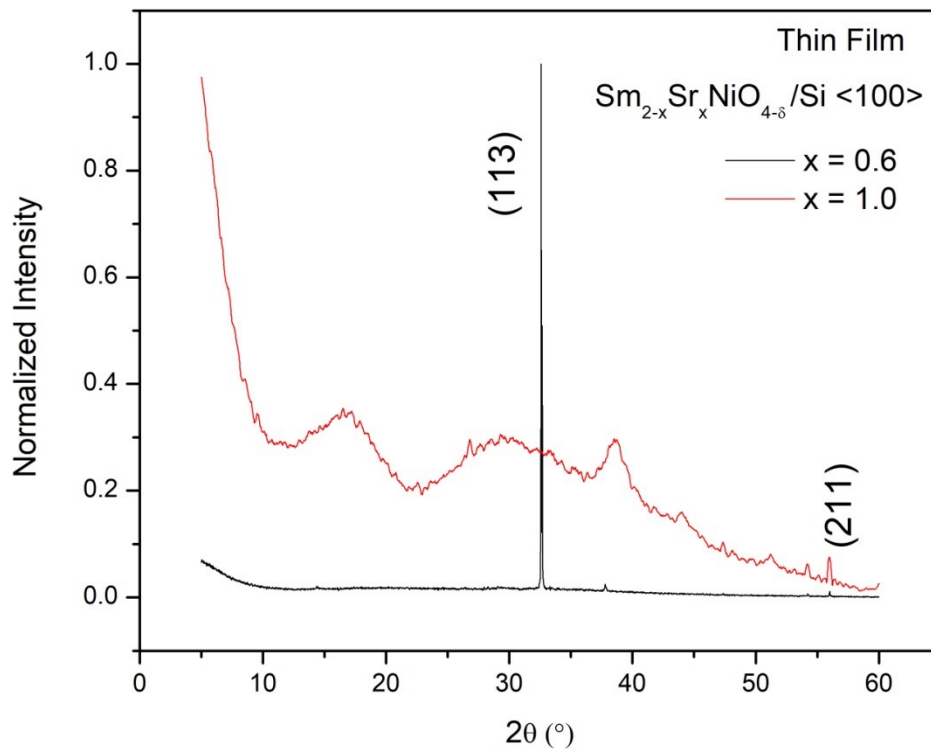


Fig.S7 depicts the X-ray diffractograms of the thin films of  $\text{Sm}_{2-x}\text{Sr}_x\text{NiO}_{4-\delta}$  ( $x = 0.6$  and  $x = 1$ ) samples

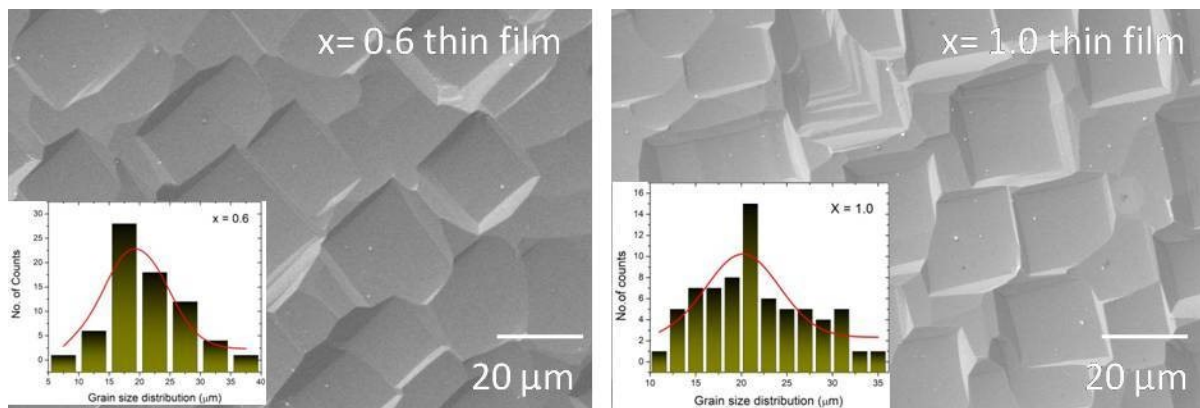


Fig. S8 SEM micrographs and respective grain size histograms for the thin films of  $\text{Sm}_{2-x}\text{Sr}_x\text{NiO}_{4-\delta}$  ( $x = 0.6, 1.0$ )

The microstructure and chemical composition of thin film of samples 0.6 and 1.0 are also characterized by SEM and EDX analysis

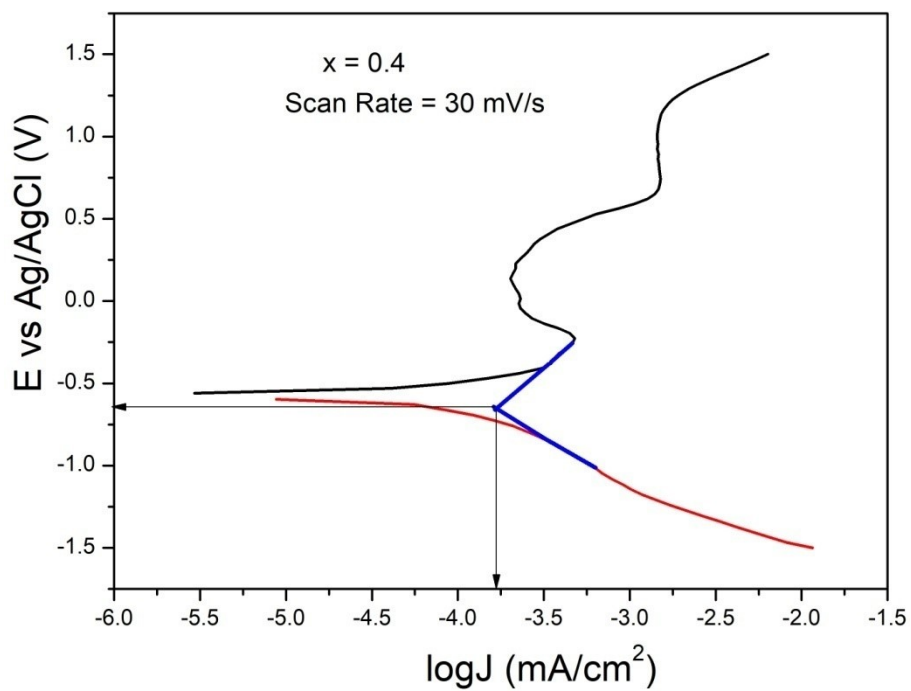


Fig.S9 Tafel slope  $E$  vs  $\text{Ag/AgCl}$  (V) and  $\log J$  ( $\text{mA/cm}^2$ ) of bulk  $\text{Sm}_{2-x}\text{Sr}_x\text{NiO}_{4-\delta}$  ( $x = 0.4$ ).

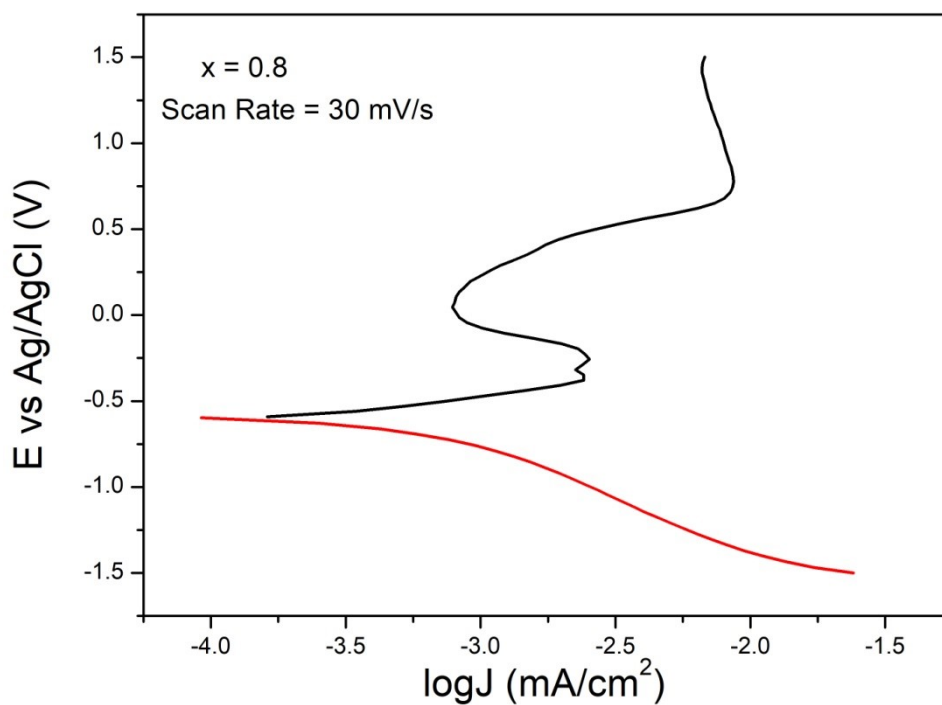


Fig.S10 Tafel slope  $E$  vs  $\text{Ag/AgCl}$  (V) and  $\log J$  ( $\text{mA/cm}^2$ ) of bulk  $\text{Sm}_{2-x}\text{Sr}_x\text{NiO}_{4-\delta}$  ( $x = 0.8$ ).

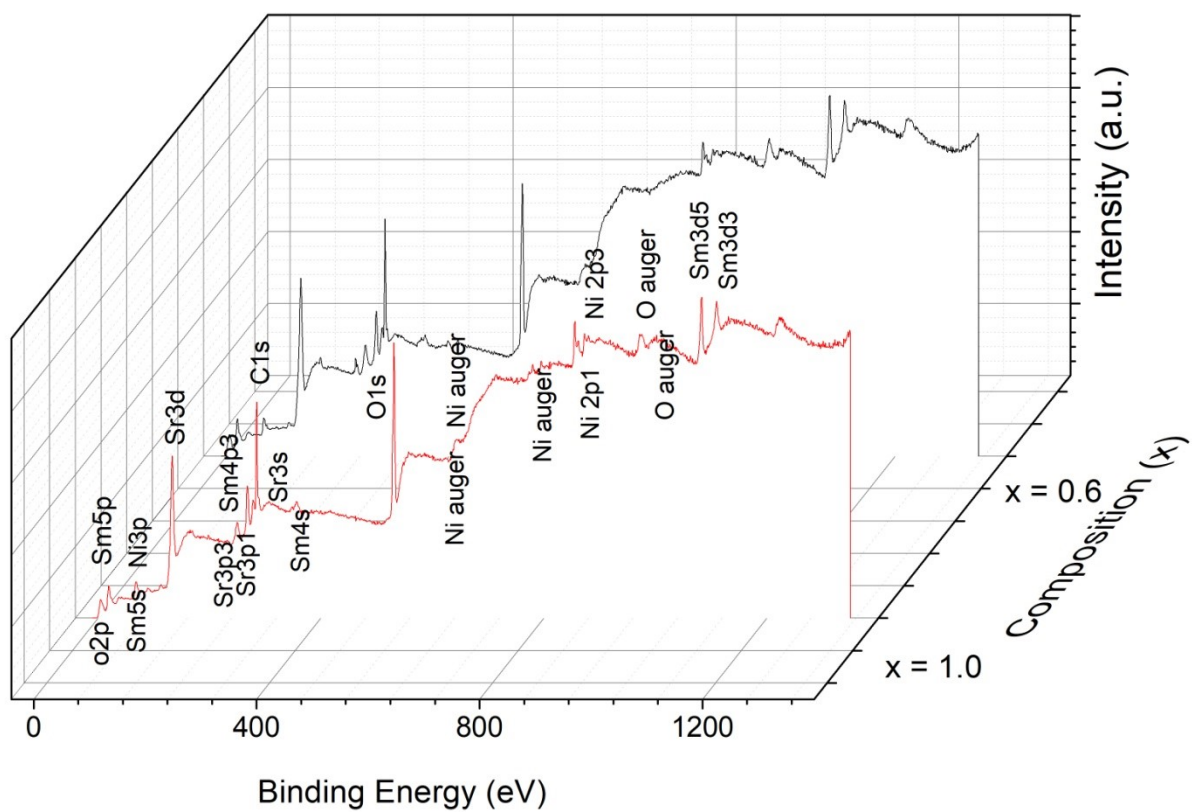


Fig.S11 Wide XPS spectra of the bulk  $\text{Sm}_{2-x}\text{Sr}_x\text{NiO}_{4-\delta}$  ( $x = 0.6$  and  $1.0$ ).